ChemComm

COMMUNICATION

View Article Online
View Journal | View Issue

Cite this: *Chem. Commun.*, 2021, 57, 6416

Received 9th February 2021,
Accepted 26th May 2021

DOI: 10.1039/d1cc00756d

rsc.li/chemcomm

A new photoelectrochemical biosensor based on FeOOH and exonuclease III-aided dual recycling signal amplification for HPV-16 detection†

Yanlin Wang, Lingying Xia, Xuelian Xiang, Ruo Yuan * and Shaping Wei*

Herein, based on iron oxyhydroxide (FeOOH) as the photoactive material and exonuclease III (exo III)-aided dual recycling signal amplification, a new photoelectrochemical (PEC) biosensor was successfully developed for human papillomavirus-16 (HPV-16) detection with a wide linear range from 0.5 fM to 1 nM and a low detection limit of 0.17 fM.

Human papillomavirus (HPV) infection is primarily responsible for cervical cancer, which is one of the most common cancers in women around the world.[1–3] High-risk genotypes of HPV, especially HPV-16 and HPV-18, are the major cause of cervical cancer worldwide.[4–6] In the past few years, some analytical methods have been applied to detect HPV, including southern blotting, colorimetry, and microarray and fluorescence analyses.[7–10] However, these methods still suffer from low sensitivity, complex preparation and high cost. Therefore, it is significantly important to develop a new method for HPV detection with high sensitivity, simple operation and low cost.

Recently, the photoelectrochemical (PEC) analytical technique in virtue of its low background, facile operation and high sensitivity has exerted a significant effect on bioanalysis owing to the separation of the light source and detection signal.[11–13] It is indispensable to exploit superior photoactive materials and effective signal amplification strategies in the construction of PEC biosensors.[14,15] So far, Cd/Pb-containing QDs have been intensively employed as photoactive materials due to their unique photophysical properties.[16,17] However, most of them are toxic and unstable, which were unfavorable for their bioassay application.[18–20] Iron oxyhydroxide (FeOOH) is an ideal material with low cost, good photostability and water solubility, natural abundance and environmental friendliness, and has been extensively applied in organic pollutant degradation and photocatalytic water oxidation, and used in electrode materials, lithium–sulfur batteries, *etc.*[21–24] More importantly, FeOOH displays a strong absorption ability in the visible light region[25] with excellent film-forming properties, which makes it suitable as a promising photoactive material for the development of a PEC biosensor. In recent years, the exonuclease III (exo III)-aided recycling amplification strategy has attracted much attention due to its low cost and simple operation, and has been widely used in the biosensing field for improving the detection sensitivity of biosensors.[26–28] Consequently, taking advantage of the features of FeOOH and the effective signal amplification strategy of exo III-aided recycling, it is highly desirable to construct a sensitive PEC biosensor for biomarker detection.

Herein, a new PEC biosensor for the detection of HPV-16 was constructed on the basis of FeOOH as the photoactive material and the exo III-aided dual recycling signal amplification strategy. As illustrated in Scheme 1, FeOOH was first added dropwise on the glassy carbon electrode (GCE) surface, leading to an obviously high initial PEC signal. At the same time, dual recycling amplification reactions (cycle I and cycle II) were triggered by exo III in the presence of a target, generating abundant single-stranded DNA (S1) to hybridize with hairpin DNA2 (HP2) on the electrode surface, thereby a large number of signal probe labeled-SiO_2 NPs (SP-SiO_2 NPs) could further hybrid with HP2, making the PEC signal obviously decreased because of the increased steric hindrance. Thus, the fabricated PEC biosensor could achieve the sensitive detection of HPV-16, displaying its potential for application in early clinical diagnosis.

The exo III-aided dual recycling signal amplification is schematically demonstrated in Scheme 1B. In the presence of the target (pink strand), it could hybridize with the protruding 3′-terminus (the green part) of hairpin DNA1(HP1) to form an HP1-Target hybrid duplex with a blunt 3′-terminus of HP1.

Key Laboratory of Luminescence Analysis and Molecular Sensing (Southwest University), Ministry of Education, College of Chemistry and Chemical Engineering, Southwest University, Chongqing 400715, P. R. China.
E-mail: yuanruo@swu.edu.cn, shapingw@swu.edu.cn;
Fax: +86-23-68253172; Tel: +86-23-68252277

† Electronic supplementary information (ESI) available: Experimental details, PAGE analysis, other characterization methods of FeOOH, optimization of experimental conditions, SEM characterization of the electrode surface, recovery test of HPV-16 in serum and Tables S1–S3. See DOI: 10.1039/d1cc00756d

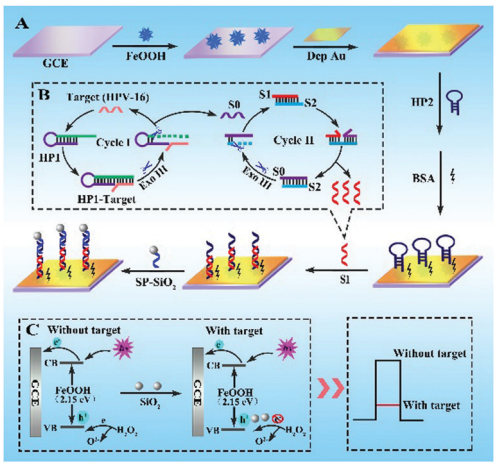

Scheme 1 Schematic illustration of the proposed PEC biosensor: (A) biosensor construction process; (B) exo III-aided dual recycling signal amplification; (C) the photocurrent generation mechanism and signal comparison.

Then exo III could specifically digest the duplex region from the 3′-terminus of HP1 in the 3′ to 5′ direction. After the duplex region was fully consumed, the target could be released to participate in the next cleavage process (cycle I) and the S0 (the purple part of HP1) could be obtained to trigger the next new recycle process (cycle II). The S1–S2 hybrid duplex was initially prepared in the solution by hybridizing S1 (red strand) and S2 (blue strand). When the S1–S2 hybrid duplex was mixed with the obtained S0, S0 could hybridize with S2 to release the free S1 and further form a new hybrid duplex (S0–S2) with a blunt 3′-terminus of S2, and then exo III could catalyze the cleavage of the hybrid duplex, releasing again S0 to launch the next cycle (cycle II). After many cycles, numerous S1 could be obtained to participate in the following experiments. It is worth noticing that the S1–S2 hybrid duplex was specifically designed with an overhang 3′-terminus for each to avoid the exo III-catalyzed digestion of them.

First, the morphologies of the FeOOH and SiO_2 NPs were characterized using scanning electron microscopy (SEM). As shown in Fig. 1A–C, FeOOH was composed of well-defined nanorods that tended to be a 3D flower-like morphology.[29]

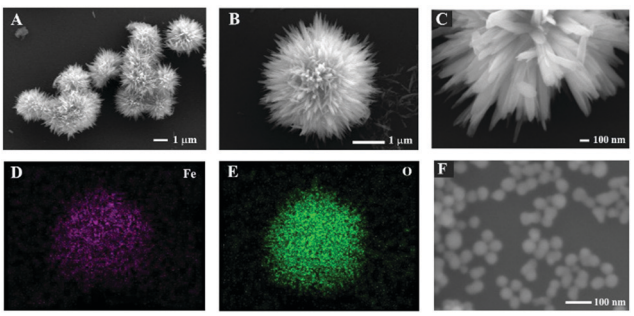

Fig. 1 (A) Overall and (B and C) magnified SEM images of FeOOH. (D and E) The corresponding elemental mapping of Fe and O for (B), respectively. (F) SEM of SiO_2 NPs.

Moreover, as shown in Fig. 1D and E, elemental mapping revealed that Fe and O were all uniformly distributed across the whole particle. Besides, as shown in Fig. 1F, the SiO_2 NPs were well dispersed with an average size of about 40 nm, which is in agreement with the previous literature.[30]

Next, Fig. 2A shows the ultraviolet-visible (UV-vis) absorption spectrum of FeOOH, which exhibited a distinct absorption band in the visible light range, suggesting that FeOOH had a good capacity for light absorption. Besides, from the equation of a direct-gap semiconductor: $(\alpha h\nu)^2 = C(h\nu - E_g)$ (α, h, ν, C and E_g represents the absorption coefficient, Planck constant, light frequency, a constant and band gap energy, respectively),[31] the E_g of FeOOH could be calculated. As shown in Fig. 2B, the E_g of FeOOH was estimated to be 2.15 eV.

In addition, X-ray photoelectron spectroscopy (XPS) was used to investigate the chemical states of different bonded elements of FeOOH. The full survey spectrum shown in Fig. 3A shows the coexistence of Fe and O and the distinct characteristic peaks. As shown in Fig. 3B, the peaks at 711.1 eV and 724.9 eV in the Fe 2p spectrum were associated with typical Fe $2p_{3/2}$ and Fe $2p_{1/2}$ in FeOOH, respectively. Besides, two shake-up satellites were also observed at 719.1 eV and 733.2 eV, due to the presence of iron in the trivalent oxidation state.[32] Moreover, the O 1 s scan spectrum displayed in Fig. 3C is divided into two different peaks at 530.0 eV and 531.3 eV, respectively. In addition, the valence band (VB) of FeOOH was measured to be 1.85 eV using the XPS VB spectrum (Fig. 3D). Based on the E_g value of FeOOH of 2.15 eV, the conduction band (CB) edge position was calculated to be −0.3 eV, according to the formula: $E_{VB} = E_{CB} + E_g$.[33] The above results suggested that FeOOH was successfully synthesized and the relatively narrow band gap of FeOOH could lead to more efficient utilization of the visible light, which makes it potentially applicable in a PEC biosensor as an ideal photoactive material.

The building process of the PEC biosensor could be characterized *via a* PEC signal. As displayed in Fig. 4A, almost no PEC signal was observed for the bare GCE (curve a). After the immobilization of FeOOH, an obviously enhanced PEC signal could be obtained (curve b) owing to the superior photoelectric activity of FeOOH. When the Au NPs were electrodeposited onto the electrode surface (Dep Au), the PEC signal obviously increased (curve c) on account of the excellent conductivity of Au NPs. After the successful incubation of HP2 and 1% BSA on the above electrode, the PEC signal gradually decreased (curves d and e)

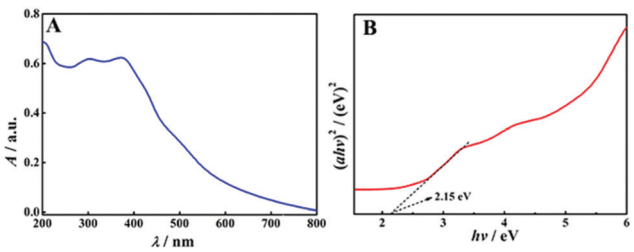

Fig. 2 (A) Typical UV-vis absorption spectrum and (B) plot of the $(\alpha h\nu)^2$ *vs.* ($h\nu$) of FeOOH.

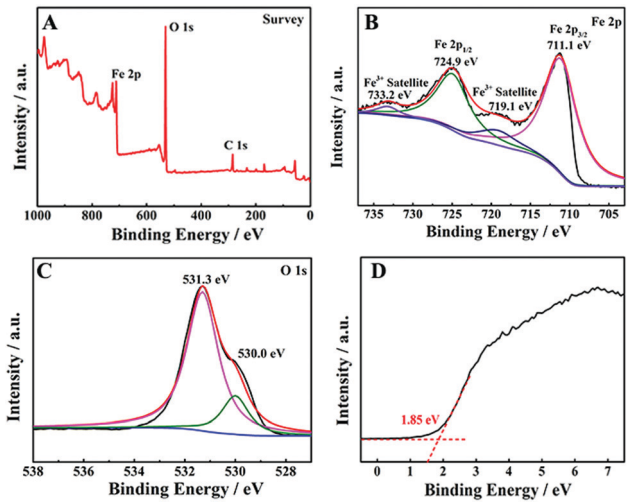

Fig. 3 (A) Full-scale XPS spectra of FeOOH. (B and C) High-resolution XPS spectra of FeOOH: Fe 2p and O 1s. (D) XPS VB spectra of FeOOH.

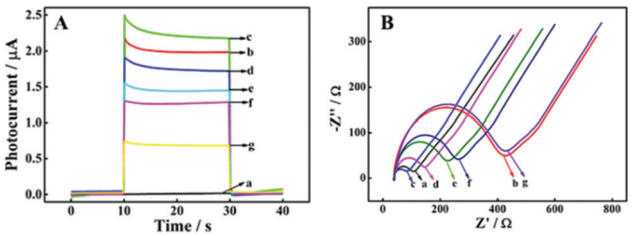

Fig. 4 (A) PEC and (B) EIS responses of (a) bare GCE; (b) FeOOH/GCE; (c) Dep Au/FeOOH/GCE; (d)HP2/Dep Au/FeOOH/GCE; (e) 1% BSA/HP2/Dep Au/FeOOH/GCE; (f) S1/1% BSA/HP2/Dep Au/FeOOH/GCE; (g) SP-SiO_2 NPs/S1/1% BSA/HP2/Dep Au/FeOOH.

because of their increased steric hindrance effect. And then the PEC signal sequentially decreased (curve f) after incubating the obtained S1 products. Finally, with the addition of SP-SiO_2 NPs, the PEC signal further decreased (curve g), because the SiO_2 NPs could impede the electron transfer and increase the steric hindrance. These results suggested that the biosensor was conceivably fabricated.

Electrochemical impedance spectroscopy (EIS) was also propitious to confirm the stepwise modification process. Fig. 4B exhibits the impedance change of each fabrication step. The bare GCE displayed a small resistance (R_{et}) value (curve a). When FeOOH was further modified on the bare GCE, the R_{et} value greatly increased (curve b) because of the large repulsion between $[Fe(CN)_6]^{3-/4-}$ and FeOOH. After the deposition of Au NPs on the modified electrode (Dep Au), the R_{et} value clearly decreased (curve c), suggesting that Au NPs could facilitate the electron transfer. With the stepwise modification of HP2, 1% BSA and the obtained S1 products, the R_{et} value consecutively increased (curves d–f) owing to their non-conductivity characteristics. Ultimately, the R_{et} value markedly increased (curve g) with the assembly of SP-SiO_2 NPs due to the poor conductivity of SiO_2 NPs. These results demonstrated that the biosensor was effectively constructed.

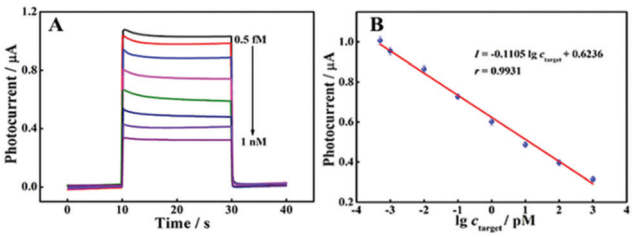

Fig. 5 (A) PEC responses of the biosensor incubated with different concentrations of the target: 0.5 fM, 1 fM, 10 fM, 100 fM, 1 pM, 10 pM, 100 pM and 1 nM (from top to bottom). (B) The corresponding calibration curve for target detection.

Under the optimal conditions, the PEC responses of the proposed method with different concentrations of the target were obtained. As seen from Fig. 5A, the PEC signals (I) accordingly decreased as the concentration (c) of the target increased from 0.5 fM to 1 nM. As shown in Fig. 5B, the linear regression equation was $I = -0.1105 \lg c + 0.6236$, $r = 0.9931$. The limit of detection was calculated to be 0.17 fM estimated at a signal-to-noise ratio of 3. The results suggested that the PEC biosensor exhibited very desirable analytical performance for HPV-16 detection. In addition, the constructed PEC biosensor in the detection of HPV-16 was compared to that found in the existing work (Table S3, ESI†), which indicated that the designed PEC biosensor exhibited a satisfactory analytical performance for HPV-16 detection owing to the excellent properties of FeOOH and exo III-aided dual recycling signal amplification strategy.

The selectivity of this method was investigated by assaying the interfering substance including single-base mismatched DNA (1c), three-base mismatched DNA (3c) and random DNA (random). As exhibited in Fig. 6A, the target (1 pM) exhibited a lower PEC signal, while the blank sample and other interfering substances (the concentration of each interfering substance, 100 pM) showed a relatively higher PEC signal, respectively. These indicated that the developed PEC biosensor possessed a high selectivity. Meanwhile, the stability of the proposed PEC biosensor was evaluated by testing the PEC signals under several continuous "on/off" irradiation cycles. As shown in Fig. 6B, the relative standard deviation (RSD) is 1.54%, demonstrating that the PEC biosensor has an acceptable stability.

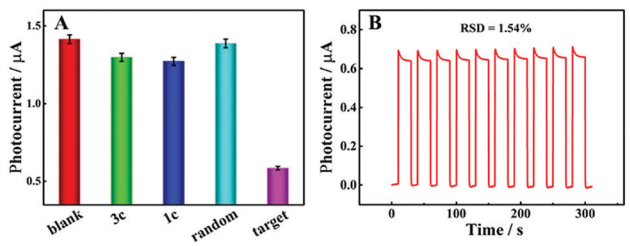

Fig. 6 (A) Selectivity of the proposed strategy toward the blank sample, three interferents (the concentration of each interferent, 100 pM) and the target (1 pM). (B) The stability of the proposed PEC biosensor incubated with 1 pM target under several "on/off" irradiation cycles.

In summary, depending on FeOOH as the photoactive material and exo III-aided dual recycling signal amplification, a new PEC biosensing platform has been proposed for HPV-16 detection. Herein, FeOOH was used as a sensing matrix that integrated the advantages of nontoxicity, easy preparation, stable chemical properties and excellent photoelectric activity for providing a stable and commendable initial photocurrent signal for the PEC biosensor. Moreover, exo III-aided dual recycling signal amplification further enhanced the detection sensitivity of the PEC biosensor. The designed PEC biosensor exhibited a wide linear range, good selectivity and satisfactory stability, proving to be potential for application in early cancer diagnosis.

This work was financially supported by the National Natural Science Foundation of China (21775124 and 21974108) and the Fundamental Research Funds for the Central Universities (XDJK2020TY002), China.

Conflicts of interest

There are no conflicts to declare.

Notes and references

1 L. J. P. Liebenberg, L. R. McKinnon, N. Yende-Zuma, N. Garrett, C. Baxter, A. B. M. Kharsany, D. Archary, A. Rositch, N. Samsunder, L. E. Mansoor, J. A. S. Passmore, S. S. A. Karim and Q. A. Karim, *Nat. Commun.*, 2019, **10**, 5227.
2 G. Sher, N. A. Salman, M. Kulinski, R. A. Fadel, V. K. Gupta, A. Anand, S. Gehani, S. Abayazeed, O. Al-Yahri, F. Shahid, S. Alshaibani, S. Hassan, M. Z. Chawdhery, G. Davies, S. Dermime, S. Uddin, G. H. Ashrafi and K. Junejo, *Cancers*, 2020, **12**, 1528.
3 R. J. Wang, W. Pan, L. Jin, W. M. Huang, Y. H. Li, D. Wu, C. Gao, D. Ma and S. J. Liao, *Cancer Lett.*, 2020, **471**, 88–102.
4 B. Zhu, Y. Z. Xiao, M. Yeager, G. Clifford, N. Wentzensen, M. Cullen, J. F. Boland, S. Bass, M. K. Steinberg, T. Raine-Bennett, D. Lee, R. D. Burk, M. Pinheiro, L. Song, M. Dean, C. W. Nelson, L. Burdett, K. Yu, D. Roberson, T. Lorey, S. Franceschi, P. E. Castle, J. Walker, R. Zuna, M. Schiffman and L. Mirabello, *Nat. Commun.*, 2020, **11**, 886.
5 C. de Martel, M. Plummer, J. Vignat and S. Franceschi, *Int. J. Cancer*, 2017, **141**, 664–670.
6 J. Y. Mao, H. W. Li, S. C. Wei, S. G. Harroun, M. Y. Lee, H. Y. Lin, C. Y. Chung, C. H. Hsu, Y. R. Chen, H. J. Lin and C. C. Huang, *ACS Appl. Mater. Interfaces*, 2017, **9**, 44307–44315.
7 M. Poljak, B. J. Kocjan, A. Ostrbenk and K. Seme, *J. Clin. Virol.*, 2016, **76**, S3–S13.
8 P. Teengam, W. Siangproh, A. Tuantranont, T. Vilaivan, O. Chailapakul and C. S. Henry, *Anal. Chem.*, 2017, **89**, 5428–5435.
9 A. Qureishi, T. Mawby, L. Fraser, K. A. Shah, H. Møller and S. Winter, *Eur. Arch. Otorhinolaryngol.*, 2017, **274**, 2675–2683.
10 X. Y. Peng, Y. L. Zhang, D. T. Lu, Y. J. Guo and S. J. Guo, *Sens. Actuators, B*, 2019, **286**, 222–229.
11 F. F. Lu, L. M. Yang, T. Hou and F. Li, *Chem. Commun.*, 2020, **56**, 11126–11129.
12 D. Long, M. J. Li, H. H. Wang, H. J. Wang, Y. Q. Chai, Z. H. Li and R. Yuan, *Anal. Chem.*, 2020, **92**, 14769–14774.
13 W. C. Geng and R. Y. Yang, *Chem. Commun.*, 2020, **56**, 2909–2912.
14 S. P. Wang, F. F. Wang, C. P. Fu, Y. N. Sun, J. G. Zhao, N. Li, Y. Q. Liu, S. G. Ge and J. H. Yu, *Anal. Chem.*, 2020, **92**, 7604–7611.
15 L. X. Meng, M. Y. Liu, K. Xiao, X. H. Zhang, C. C. Du and J. H. Chen, *Chem. Commun.*, 2020, **56**, 8261–8264.
16 R. Xu, Y. Du, D. Q. Leng, L. Liu, Y. Y. Li, X. Ren, D. W. Fan, H. Wang and Q. Wei, *Chem. Commun.*, 2020, **56**, 7455–7458.
17 G. L. Wang, F. Yuan, T. Gu, Y. Dong, Q. Wang and W. W. Zhao, *Anal. Chem.*, 2018, **90**, 1492–1497.
18 Q. Zhou, H. j. Xue, Y. Y. Zhang, Y. Q. Lv, H. G. Li, S. Q. Liu, Y. F. Shen and Y. J. Zhang, *ACS Sens.*, 2018, **3**, 1385–1391.
19 S. S. Liu, H. J. Cao, Z. Y. Wang, W. W. Tu and Z. H. Dai, *Chem. Commun.*, 2015, **51**, 14259–14262.
20 C. Q. Zhao, J. Zhou, K. W. Wu, S. N. Ding, J. J. Xu and H. Y. Chen, *Anal. Chem.*, 2020, **92**, 6886–6892.
21 X. F. Qian, Y. W. Wu, M. Kan, M. Y. Fang, D. T. Yue, J. Zeng and Y. X. Zhao, *Appl. Catal., B*, 2018, **237**, 513–520.
22 G. Ge, M. Liu, C. Liu, W. Zhou, D. F. Wang, L. Q. Liu and J. H. Ye, *J. Mater. Chem. A*, 2019, **7**, 9222–9229.
23 K. L. Li, X. Y. Liu, T. X. Zheng, D. B. Jiang, Z. Zhou, C. Q. Liu, X. M. Zhang, Y. X. Zhang and D. Losic, *Chem. Eng. J.*, 2019, **370**, 136–147.
24 B. B. Wei, C. Q. Shang, X. Wang and G. F. Zhou, *Small*, 2020, **16**, 2002789.
25 T. Q. Wang, Z. F. Jiang, K. H. Chu, D. Wu, B. Wang, H. L. Sun, H. Y. Yip, T. C. An, H. J. Zhao and P. K. Wong, *ChemSusChem*, 2018, **11**, 1365–1373.
26 X. M. Qu, D. Zhu, G. B. Yao, S. Su, J. Chao, H. J. Liu, X. L. Zuo, L. H. Wang, J. Y. Shi, L. H. Wang, W. Huang, H. Pei and C. H. Fan, *Angew. Chem., Int. Ed.*, 2017, **56**, 1855–1858.
27 Z. C. Chen, F. Xiong, A. M. Yu and G. S. Lai, *Chem. Commun.*, 2019, **55**, 3959–3962.
28 X. B. Huang, S. H. Wu, H. C. Hu and J. J. Sun, *ACS Sens.*, 2020, **5**, 2636–2643.
29 S. Agarwala, Z. H. Lim, E. Nicholsonb and G. W. Ho, *Nanoscale*, 2012, **4**, 194–205.
30 H. H. Wang, M. J. Li, Y. N. Zheng, T. Hu, Y. Q. Chai and R. Yuan, *Biosens. Bioelectron.*, 2018, **120**, 71–76.
31 W. Zhao, Y. Liu, Z. Wei, S. Yang, H. He and C. Sun, *Appl. Catal., B*, 2016, **185**, 242–252.
32 J. Q. Liu, M. B. Zheng, X. Q. Shi, H. B. Zeng and H. Xia, *Adv. Funct. Mater.*, 2016, **26**, 919–930.
33 J. Shu and D. P. Tang, *Anal. Chem.*, 2020, **92**, 363–377.